European Journal of Electrical Engineering
Vol. 22, No. 1, February, 2020, pp. 57-62
Journal homepage: http://iieta.org/journals/ejee

Design and Application of a Visualized Fault Joint Diagnosis System for Overheating Fault of Gas Insulated Switchgear

Bo Li[1*], Lei Fan[1], Yingxia Liu[2], Jinhang He[1], Bo Sun[1]

[1] Electric Power Research Institute of Guizhou Power Grid Co., Ltd., Guiyang 550002, China
[2] Guizhou Communications Polytechnic, Guiyang 550008, China

Corresponding Author Email: Libo@gcp.edu.cn

https://doi.org/10.18280/ejee.220107

Received: 10 September 2019
Accepted: 27 November 2019

Keywords:
gas-insulated switchgear (GIS), overheating fault, X-ray, visualized fault, joint diagnosis system

ABSTRACT

Aiming at the low accuracy of traditional gas-insulated switchgear (GIS) fault diagnosis systems in internal fault and over-heating fault diagnosis, this study designed a novel automatic fault diagnosis system for GIS based on support vector machine (SVM) and X-ray technology. The hardware of the system uses DSP core processor to process the data, it consists of a multi-channel sensor module, a network data communication module, a portable X-ray flaw detector, and other parts; The software of the system uses SVM to construct an online diagnosis module and achieve visualized and automatic diagnosis of busbar joint overheating fault and visual metal contacts fault, etc. After the introduction of the system, this study conducted a comparative experiment on the proposed system and the traditional system, and the results showed that the proposed system outperformed the traditional system by 35% in the accuracy rate of high-temperature overheating fault diagnosis; while in terms of medium-and-low temperature overheating fault diagnosis, this number was 22%; meanwhile, field application also showed that the X-ray-based visualized fault diagnosis system played a crucial role in the fault identification of disconnectors and circuit breakers in many 110kV/220kV substations.

1. INTRODUCTION

With the application and promotion of new technologies such as anti-interference transmission and microprocessors, studies on the fault diagnosis of GIS busbar joints overheating have gradually increased, for example, many scientific research institutions have developed various monitoring systems such as the online switchgear monitoring system [1-4], monitoring system for dissolved gas in oil [5-7], and online monitoring system for power generation equipment [8-10]. The successful development of these systems has improved the traditional methods which have to shut down the equipment before detecting and diagnosing faults in GIS, these new systems have realized real-time monitoring of GIS [11, 12], making the automatic diagnosis of GIS busbar joints overheating failure possible, which is also conductive to data storage and manpower saving. Moreover, with the advancement of high tech, some new methods have applied to the field of fault diagnosis, such as pattern recognition, nonlinear theory, data mining algorithms, wavelet transforms, and principal component analysis, etc., all these methods have been widely applied in the diagnosis of busbar joint overheating failure, and the diagnosis systems of such failure have developed rapidly as well. The traditional busbar joint overheating fault diagnosis systems mainly adopt the data mining technology, which searches for rules in the sample data and infers the overall data based on the found rules [13]. For different requirements, data mining technology can mine different inferences and descriptions in a same set of data. Due to the low accuracy of the traditional busbar joint overheating fault diagnosis systems, this study designed a novel GIS busbar joint overheating fault automatic diagnosis system based on SVM (hereinafter referred to as the proposed system). SVM is a machine learning method based on the principle of structural risk minimization and the theory of statistical learning, it builds data models to conduct statistical pattern recognition and could obtain good results with limited data samples. In addition, the proposed system also adds a portable X-ray machine, which uses X-ray technology to judge the visualized fault conditions insides the GIS, and further improves the diagnostic accuracy of the equipment.

This paper firstly introduced the hardware design of the fault automatic diagnosis system, Then, the comparative experiment between the automatic fault diagnosis system and the traditional bus joint overheat fault diagnosis system was carried out, Finally, the practical cases of the diagnosis system in the fault discrimination of disconnectors and breakers in 110kV / 220kV substations are analyzed.

2. HARDWARE DESIGN

The hardware of the proposed system includes: a core processor module, a network data communication module, and a multi-channel sensor module [14].

2.1 Design of the multi-channel sensor module

The multi-channel sensor module contains two types of sensors: one is used for qualitative feature detection, it consists of a hydrogen sensor and a carbon monoxide sensor, and it is installed inside the oil conservator air chamber of the GIS; the other is used for quantitative feature detection, actually it is a temperature and humidity sensor installed in the circulating cooling system of the GIS. With the help of the two types of sensors, we can collect data signals at the busbar joints of GIS, including temperature signals, humidity signals, hydrogen signals, and carbon monoxide signals, etc. [15], wherein the temperature and humidity sensor is the most important part for the diagnosis of overheating faults. The proposed system adopted the SHTCI digital temperature and humidity sensor which is a kind of smart sensor and supports mobile devices, this sensor is the smallest-volume temperature and humidity sensor developed under the current technology, it integrates the analog signal processing circuits and the temperature and humidity sensor components on a microchip, and both its operating voltage and power consumption are very low.

The model TSG228FT hydrogen sensor was adopted as the hydrogen sensor in the proposed system to ensure good hydrogen sensitivity. When hydrogen appears, the conductivity of the sensor will increase with the hydrogen concentration, and the model TSG228FT hydrogen sensor can convert the change in the conductivity to the hydrogen concentration signal and output the signal. Meanwhile, the model LMP1277 carbon monoxide sensor was adopted as the carbon monoxide sensor in the proposed system, when there's carbon monoxide at the position of the busbar joints, the sensor signal will be enhanced. The output signal frequency range of model LMP1277 carbon monoxide sensor is 100-100Hz, and the corresponding gas volume fraction is $0\text{-}10^{-3}$, which can flexibly detect the volume of the carbon monoxide.

2.2 Design of the core processor module

For the core processor module, the 3215DSP core processor was taken as the main processor of the proposed system, and the TMS231F32x chip was adopted for data processing. The 3215DSP core processor has low power consumption and high performance, it supports JATG boundary scan and has 32-bit high-performance central processor, serial peripheral interface (SPI) mode, 16 CDA conversion interface channels, 2 serial communication interfaces (SCI), and multi-channel buffered serial ports (BSP); it also has multi-purpose transmission pins, compared with the traditional busbar joint overheating fault diagnosis systems, this core processor increases the data processing rate of the proposed system, and thereby improving the diagnostic accuracy of the proposed system. The flash programmable voltage of the power circuit of the core processor module is 3.5V, the system I/O output power and input power are both 3.2V, and the chip's internal and external power supply and core power supply are all 1.7V; the system has six sets of power input: Analog 3.5V, Analog 3.2V, Analog 1.7V, Digital 3.5V, Digital 3.2V, and Digital 1.7V. The ML7111 and ML7113 power management chips were used to design the 32x chip, the output voltage accuracy of these two power management chips is relatively high, so they can give about 1A output current to the 32x chip. The power supply circuit of the core processor module is shown in Figure 1. The 32x chip can be directly connected to the digital power supply pin of the 3215DSP core processor through the output voltage.

For the core processor module, we also need to design a JATG interface for program testing and chip download, and this JATG interface consists of boundary scan interface, EMUI extension interface, EMUO extension interface, and IEEE standard protocol test interface. Moreover, in order to convert all external input analog signals into digital signals, we also need to design a CDA conversion interface. The CDA in the 3215DSP core processor is a pipeline-structured high-resolution analog-to-digital converter, so the CDA conversion interface adopted two 8-channel multiplexers (MUX), and there's a total of 16 channels, which can help the analog-to-digital converter to quickly convert the signals in the core processor module. The peripheral connection of the CDA conversion interface is shown in Figure 2.

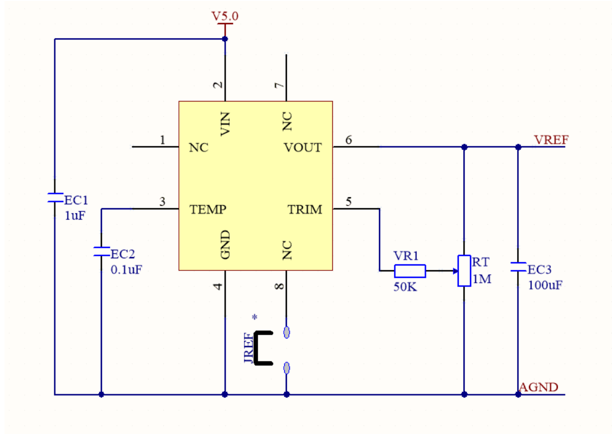

Figure 1. Power supply circuit of core processor module

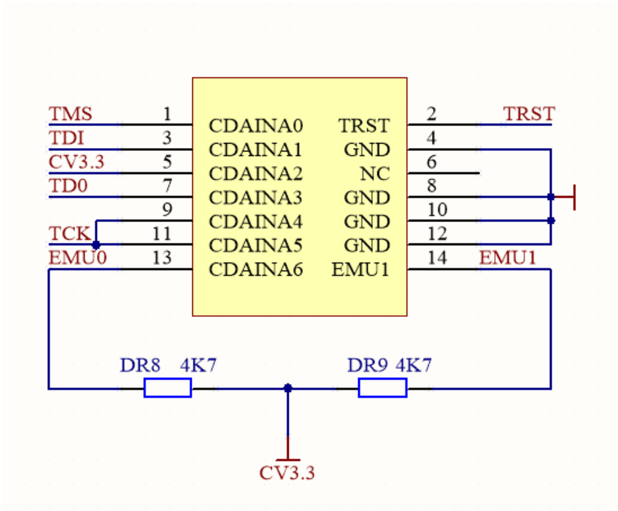

Figure 2. Peripheral connection of CDA conversion interface

2.3 Design of the network data communication module

The network data communication module can support short messaging service (SMS), fax, data, voice mail and other services. It is highly integrated and has a compact structure, it supports both high and low temperature working environments, and consumes less current. The power supply voltage of this module is 3.2V-4.9V, the module is mainly composed of an application interface, a baseband controller and a radio frequency (RF) device. The baseband controller can control signal amplification, conversion, and transmission, etc.; the RF device is responsible for receiving and sending analog signals; the application interface is the SCI interface, which consists of two modules, SCI1 and SCI2. Each of the two modules has a transmitter and a receiver, and each has a FIFO with a depth of 10, so that each has its own independent interrupt and enable bits, and can perform half-duplex communication and full-duplex communication separately and independently. Since serial data communication is required in the busbar joint overheating fault automatic diagnosis system, we could only use SCI interface to make connection indirectly, therefore, we designed a SR232 interface for level conversion, so as to convert the negative logic level of the SCI interface to the COMS level. The SR232 interface consists of a MAX2323 chip and a converter, and it can send and receive analog signals at the same time.

3. SVM-BASED OVERHEATING FAULT DIAGNOSIS

The automatic diagnosis of the busbar joint overheating fault needs to be conducted in the core processor module and completed by the online diagnosis module built based on SVM. SVM is used to classify signal data status so as to complete fault diagnosis. The SVM classification linear equation is shown below:

$$\omega \cdot x + b = 0 \tag{1}$$

where, ω is the classification interval; x is the classification sample; b is the training error rate. The detection indicator of the busbar joint overheating fault is p. (x_i, y_i) represents the signal data classification samples, wherein x_i is the sum of temperature and humidity data and y_i is the sum of gas data. Eq. (1) was used to classify the signal data classification samples, when:

$$x_i\left[\left(\omega \cdot y_i\right)+b\right]-1 \geq p \tag{2}$$

It indicates that there is a busbar joint overheating fault, when:

$$x_i\left[\left(\omega \cdot y_i\right)+b\right]-1 \leq p \tag{3}$$

It indicates that there is no busbar joint overheating fault. With the online diagnosis module of the joint diagnosis system, signal data processing and fault analysis could be completed.

3.1 Experimental parameters

In order to test the proposed system, this study designed a comparative experiment and the experimental parameters are shown in Table 1 below:

Table 1. Experimental parameters

Items	Data
Platform	Matlab Web platform
Fault classification	High temperature overheating, medium-and-low temperature overheating
Operation procedures	Data signal acquisition, signal conversion, signal storage, data signal classification, overheating fault diagnosis
Evaluation criteria	New structure industry with the best integration and transition effect
Measuring standard	System diagnostic accuracy
Operating system	Win10
Experimental data	High-temperature overheating fault diagnostic accuracy, medium-and-low temperature overheating fault diagnostic accuracy

3.2 Diagnosis process

The temperature signal, humidity signal, hydrogen signal, and carbon monoxide signal at the position of GIS busbar joint were collected by the hydrogen sensor, carbon monoxide sensor, and temperature and humidity sensor and taken as the experimental data, then the core processor module was used to convert the analog signals and store them, the online diagnostic module was used to analyze the experimental data and diagnose the high temperature overheating and medium-and-low temperature overheating through the signal types. To ensure the validity of the experiment, a traditional busbar joint overheating fault diagnosis system was compared with the proposed system, 300 tests were performed respectively, and the experimental results were observed.

3.3 Diagnosis results

The traditional busbar joint overheating fault diagnosis system and the proposed system were compared, the high temperature overheating fault diagnostic accuracy of the two is shown in Figure 3, and the medium-and-low temperature overheating fault diagnostic accuracy of the two is shown in Figure 4.

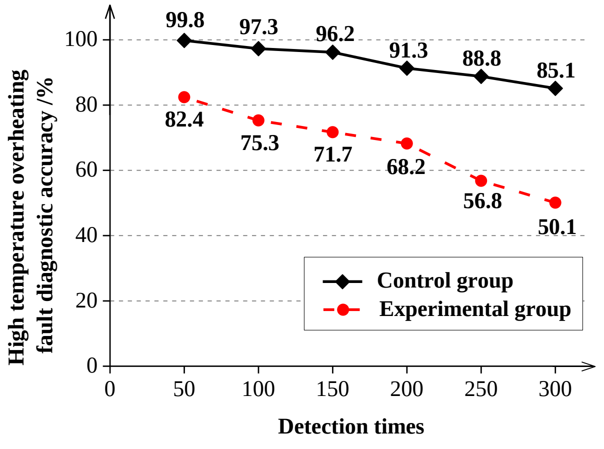

Figure 3. Comparison of high temperature overheating fault diagnostic accuracy

By comparing Figure 3 with Figure 4 we can know that, the proposed system outperformed the traditional system in high, medium and low temperature overheating fault diagnostic accuracy; after 100 times of high temperature overheating fault diagnosis, the diagnostic accuracy of the proposed system was 22% higher than the traditional system; after 200 times of high temperature overheating fault diagnosis, the diagnostic accuracy of the proposed system was 22% higher than the traditional system; after 300 times of high temperature overheating fault diagnosis, the diagnostic accuracy of the proposed system was 35% higher than the traditional system. After 100 times of medium-and-low temperature overheating fault diagnosis, the diagnostic accuracy of the proposed system was 16% higher than the traditional system; after 200 times of medium-and-low temperature overheating fault diagnosis, the diagnostic accuracy of the proposed system was 20% higher than the traditional system; after 300 times of medium-and-low temperature overheating fault diagnosis, the diagnostic accuracy of the proposed system was 22.5% higher than the traditional system.

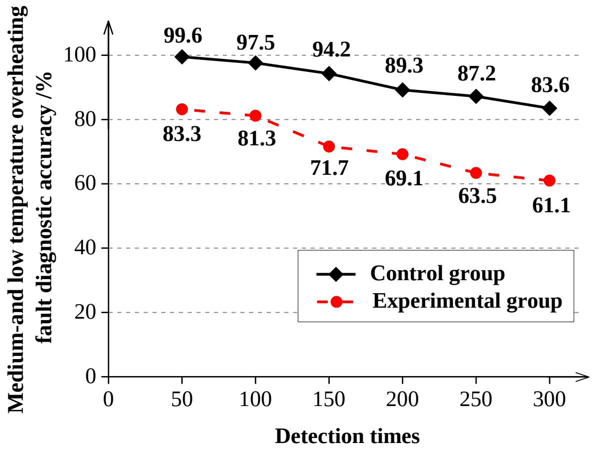

Figure 4. Comparison of medium-and-low temperature overheating fault diagnostic accuracy

4. X-RAY-BASED VISUALIZED FAULT DIAGNOSIS

The proposed system introduced a portable intelligent X-ray flaw detector [16-18], which can detect welds and defects inside the GIS, and this technology has played an important role in visualized fault monitoring of disconnectors, transmission rods and other parts of many 110kV/220kV substations. The X-ray-based visualized fault diagnosis method is a kind of non-destructive testing method, which is quite different from the conventional PD detection and ultra-high-frequency detection [19-22]. However, it should be noted that introducing X-ray-based visualized fault diagnosis to the joint diagnosis system is an innovative design which has high practical engineering value. However, in the actual operation process, it is necessary to ensure the consistency of the test angles during the tests of a same position, thereby ensuring the consistency of the photos taken multiple times, and only in this way can the visualized fault diagnosis be well performed.

Digital X-ray inspection was performed on the opening status of the disconnector and the opening/closing status of the grounding knife switch, and the inspection results showed that, under the opening disconnector conditions, there're situations in which the moving contact was protruding from the voltage-sharing hood, which might affect the normal operation of the equipment. Comparing Figure 5 and Figure 6, it can be seen that in the position pointed by the red arrow in Figure 6, the moving contact did not return to the original position under the opening status of the disconnector, it protruded from the voltage-sharing hood by 9.1mm, which posed a safety hazard. In Figure 7, the position pointed by the red arrow showed that the moving contact did not return to the original position under the opening status of the disconnector, it protruded from the voltage-sharing hood by 10.8mm, which posed a safety hazard as well.

Figure 5. Schematic diagram of flaw position and photos (normal phase)

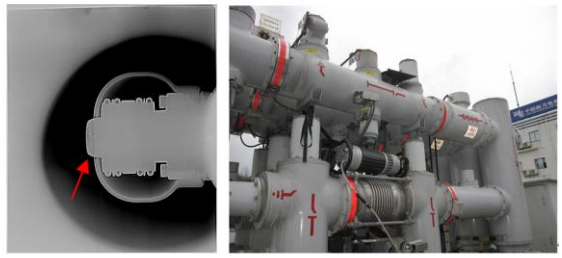

Figure 6. Schematic diagram of flaw position and photos (fault phase)

Figure 7. Schematic diagram of flaw position and photos (fault phase)

It can be seen from the X-ray inspection images of the transmission rod shown in Figure 8 that the position of the transmission rod of the fault phase was obviously deviated from that of the normal phase, the transmission rod of the fault phase had been displaced, posing a hidden safety hazard. It can be seen that the portable X-ray flaw detection technology of the proposed system played a key role in analyzing and judging the visualized faults inside the equipment.

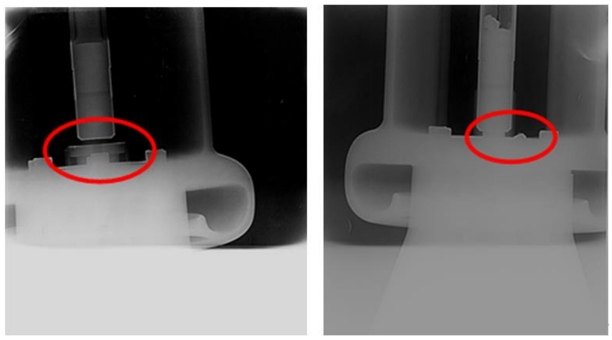

(a) Normal phase (b) Fault phase

Figure 8. Transmission rod X-ray inspection images

For a 110kV substation which had partial discharge signals, its GIS switch B-phase cable heads were subject to X-ray flaw inspection, and it's found that at the boss position, there's obvious cracks (see Figure 9); after that, the cabin was opened and disassembled (Figure 10, Figure 11, Figure 12), and it's found that no cracks, pores, or other defects were seen in the upper end of the insulated bushing in the A, B, and C directions, and cracks were found in the lower end of the insulated bushing in the D direction. When examining the material object according to the photos, it's found that there was a lump peeling off at the position of the cracks, and the peeling position was at the boss which was located at the lower end of the insulated bushing (see Figure 12), the peeling area was 40 × 15mm^2, and the maximum thickness of the lump was 8mm, so it's judged that this is the cause of the partial discharge signals.

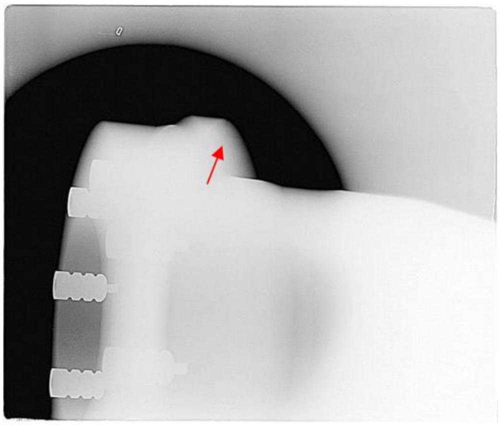

Figure 9. Schematic diagram of the flaw detection position

Figure 10. A photo of the interior of cabin

Figure 11. A photo of cable head

Figure 12. A photo of boss cracking and peeling off

5. CONCLUSION

This paper proposed a visualized fault joint diagnosis system for GIS overheating faults based on SVM and X-ray technology. In terms of high temperature overheating faults, the diagnostic accuracy of the proposed system was 35% higher than that of the traditional system; in terms of medium-and-low temperature overheating faults, the diagnostic accuracy of the proposed system was 22% higher than that of the traditional system; moreover, the visualized fault diagnosis method based on X ray can discover visual faults of metal components inside the equipment intuitively and clearly, and it has played a key role in diagnosing faults of disconnectors and circuit breakers in multiple 110kV/220kV substations. The proposed system is worthy of promotion, and it can effectively improve the safety and service life of GIS.

ACKNOWLEDGMENT

This paper is financial supported by the science and technology project of China Southern Power Grid Corporation which named 'Research on Key Technologies of digital ray intelligent diagnosis and expert consultation system for GIS equipment'.

REFERENCES

[1] Du, Y.M., Gu, N.H. (2015). Current situation and accidents of power distribution switchgear in China. High Voltage Apparatus, 37(3): 1-5.

[2] Polycarpou, A.A., Soom, A., Swarnakar, V., Valtin, R.A., Acharya, R.S., Demjanenko, V., Soumekh, M., Porter, J.W. (1996). Event timing and shape analysis of vibration bursts from power circuit breakers. IEEE Transactions on Power Delivery, 11(2): 848-857. https://doi.org/10.1109/61.489343

[3] Runde, M., Ottesen, G.E., Skyberg, B., Ohlen, M.J.I.P. (1996). Vibration analysis for diagnostic testing of circuit-breakers. IEEE Transactions on Power Delivery, 11(4): 1816-1823. https://doi.org/10.1109/61.544262

[4] Glinkowski, M.T., Schmidt, L., Veverka, E.F. (1998). Bibliography of switchgear literature. IEEE Committee Report. IEEE Transactions on Power Delivery, 13(1): 135-156. https://doi.org/10.1109/61.660872

[5] Liu, X.Y., Zhou, F.J. (2002). Research on on-line DGA with FTIR. Transformer, 39(6): 29-32.

https://doi.org/10.3969/j.issn.1001-8425.2002.06.009
[6] Jia, R.J. (1998). Development of on-line monitoring device for hydrogen dissolved in transformer oil. Power System Technology, 22(1): 4-7. https://doi.org/10.3321/j.issn:1000-3673.1998.01.002
[7] Jiang, J., Ma, G.M., Song, H.T., Zhou, H.Y., Li, C.R., Wang, H.B., Luo, Y.T., Wu, H. (2016). Tracing methane dissolved in transformer oil by tunable diode laser absorption spectrum. IEEE Transactions on Dielectrics and Electrical Insulation, 23(6): 3435-3442. https://doi.org/10.1109/TDEI.2016.005810
[8] Wang, Z.J., Xia, H.P. (2018). Influence of relationship between UHF singnals and discharge quantity of partial discharge under varius pressure in gas insulated switchgear. Electric Power Engineering Technology, 37(3): 107-111. http://dx.doi.org/10.12158/j.2096-3203.2018.03.019
[9] Cheng, L., Li, X.X., Tang, J., Zhang, C., Zhang, Y., Yao, Q. (2018). Discharge process and its mechanism analysis in flowing liquid dielectric containing metal particles at different temperatures. High Voltage Engineering, 44(9): 2917-2925. http://dx.doi.org/10.13336/j.1003-6520.hve.20180828020
[10] Teng, W., Fan, S., Gong, Z., Jiang, W., Gong, M. (2018). Fault diagnosis of transformer based on fuzzy clustering and the optimized wavelet neural network. Systems Science & Control Engineering, 6(3): 359-363. https://doi.org/10.1080/21642583.2018.1564891
[11] Wei, B., Sun, T., Wang, X.M. (2017). Application of combined acoustic and electric detection method in partial discharge detection of GIS. Electric Engineering, 6(A): 86-87, 90. http://dx.doi.org/10.3969/j.issn.1002-1388.2017.06.039
[12] Ito, T., Kamei, M., Ueta, G., Okabe, S. (2011). Improving the sensitivity verification method of the UHF PD detection technique for GIS. IEEE Transactions on Dielectrics and Electrical Insulation, 18(6): 1847-1853. https://doi.org/10.1109/TDEI.2011.6118622
[13] Men, L.Z., Li, X., Xi, L., Liu, Y.M. (2017). A Hi-Rel multi-channel DC-SSPC based on OpenVPX. Electronic Design Engineering, 25(31): 149-152. https://doi.org/10.3969/j.issn.1674-6236.2017.11.037
[14] Ma, J.P., Zhang, Y.H. (2016). Heating furnace 35 kv bus static reactive compensation device design and application. Automation & Instrumentation, 21(25): 140-142. https://doi.org/10.14016/j.cnki.1001-9227.2016.05.040
[15] Li, H.T., Shu, N.Q., Sun, G.X., Xie, Z.Y., Jin, X.C. (2014). Scale model of overheat failure in gas-insulated switchgear bus contact. Proceedings of the CSEE, 24(44): 4137-4144. https://doi.org/10.13334/j.0258-8013.pcsee.2014.24.018
[16] Jiang, W.T., Liu, R.H., Yang, Y.C., Zhang, S.Q., Chen, X.Y. (2018). The development and application of X-ray digital image size measurement software. Computer Engineering & Software, 39(5): 207-211. https://doi.org/10.3969/j.issn.1003-6970.2018.05.042
[17] Yan, B., He, X.M., Wu, T.S., Wang, Z.H., Li, S.P. (2010). X-ray visualization detection technology for GIS equipment. Electric Power, 43(7): 44-46. https://doi.org/10.3969/j.issn.1004-9649.2010.07.009
[18] Wang, D.D., Wei, J., Yu, H., Zhao, X.P., Wu, Z.Q. (2012). Nondestructive testing of GIS equipment by C-ray digital imaging. Yunnan Electric Power, 40(2): 8-10. https://doi.org/10.3969/j.issn.1006-7345.2012.02.003
[19] Gao, W., Ding, D., Liu, W., Huang, X. (2013). Analysis of the intrinsic characteristics of the partial discharge induced by typical defects in GIS. IEEE Transactions on Dielectrics & Electrical Insulation, 20(3): 782-790. https://doi.org/10.1109/TDEI.2013.6518948
[20] Gao, W., Zhao, D., Ding, D., Yao, S., Zhao, Y., Liu, W. (2015). Investigation of frequency characteristics of typical PD and the propagation properties in GIS. IEEE Transactions on Dielectrics and Electrical Insulation, 22(3): 1654-1662. https://doi.org/10.1109/TDEI.2015.7116362
[21] Okabe, S., Ueta, G., Hama, H., Ito, T., Hikita, M., Okubo, H. (2014). New aspects of UHF PD diagnostics on gas-insulated systems. IEEE Transactions on Dielectrics and Electrical Insulation, 21(5): 2245-2258. https://doi.org/10.1109/TDEI.2014.004391
[22] Zhu, M.X., Xue, J.Y., Zhang, J.N., Li, Y., Deng, J.B., Mu, H.B., Zhang, G.J., Shao, X.J., Liu, X.W. (2016). Classification and separation of partial discharge ultra-high-frequency signals in a 252 kV gas insulated substation by using cumulative energy technique. IET Science, Measurement & Technology, 10(4): 316-326. https://doi.org/10.1049/iet-smt.2015.0171